Modeling the Effects of Transcranial Magnetic Stimulation on Spatial Attention

Ying Jing[1,2], Ole Numssen[1,2], Konstantin Weise[1,3], Benjamin Kalloch[1,4], Lena Buchberger[2], Jens Haueisen[4], Gesa Hartwigsen[2,5*], Thomas R. Knösche[1,4*]

1. Methods and Development Group Brain Networks, Max Planck Institute for Human Cognitive and Brain Sciences, Stephanstraße 1a, 04103, Leipzig, Germany.

2. Lise Meitner Research Group Cognition and Plasticity, Max Planck Institute for Human Cognitive and Brain Sciences, Stephanstraße 1a, 04103, Leipzig, Germany.

3. Advanced Electromagnetics Group, Technische Universität Ilmenau, Helmholtzplatz 2, 98693, Ilmenau, Germany.

4. Institute of Biomedical Engineering and Informatics, Technische Universität Ilmenau, Gustav-Kirchhoff-Straße 2, 98693, Ilmenau, Germany.

5. Wilhelm Wundt Institute for Psychology, Leipzig University, Neumarkt 9-19, 04109, Leipzig, Germany.

Abstract

Objectives: Transcranial magnetic stimulation (TMS) has been widely used to modulate brain activity in healthy and diseased brains, but the underlying mechanisms are not fully understood. Previous research leveraged biophysical modeling of the induced electric field (E-field) to map causal structure-function relationships in the primary motor cortex. This study aims at transferring this localization approach to spatial attention, which helps to understand the TMS effects on cognitive functions, and may ultimately optimize stimulation schemes. **Approach:** Thirty right-handed healthy participants underwent a functional magnetic imaging (fMRI) experiment, and seventeen of them participated in a TMS experiment. The individual fMRI activation peak within the right inferior parietal lobule (rIPL) during a Posner-like attention task defined the center target for TMS. Thereafter, participants underwent 500 Posner task trials. During each trial, a 5-pulse burst of 10 Hz repetitive TMS (rTMS) was given

over the rIPL to modulate attentional processing. The TMS-induced E-fields for every cortical target were correlated with the behavioral modulation to identify relevant cortical regions for attentional orientation and reorientation. **Main results:** We did not observe a robust correlation between E-field strength and behavioral outcomes, highlighting the challenges of transferring the localization method to cognitive functions with high neural response variability and complex network interactions. Nevertheless, TMS selectively inhibited attentional reorienting, resulting in task-specific behavioral impairments. The BOLD-measured neuronal activity and TMS-evoked neuronal effects showed different patterns, which emphasizes the principal distinction between the neural activity being correlated with (or maybe even caused by) particular paradigms, and the activity of neural populations exerting a causal influence on the behavioral outcome. **Significance:** This study is the first to explore the mechanisms of TMS-induced attentional modulation through electrical field modeling. Our findings highlight the complexity of cognitive functions and provide a basis for optimizing attentional stimulation protocols.

Keywords

Transcranial magnetic stimulation, Electrical field, Brain mapping, Magnetic resonance imaging, Posner task, Spatial Attention

1. Introduction

Transcranial magnetic stimulation (TMS) is a non-invasive brain stimulation technique that allows the modulation of cortical function in vivo. It has been widely used to map structure-function relationships in healthy brains (Bestmann and Feredoes, 2013; Groppa et al., 2013), as well as for therapeutic application (Perera et al., 2016; Rawji et al., 2020). In brief, TMS induces an electric field (E-field) in the brain, which can temporarily excite or inhibit the stimulated area by depolarizing or hyperpolarizing cell membranes (Hallett, 2000). However, the precise location of the

neuronal populations which are affected by the induced E-field and cause the observed behavioral or physiological changes are difficult to determine. As a result, TMS studies often exhibit considerable interindividual variability in the observed outcome, which hampers its general efficacy in both basic research and clinical applications (Hartwigsen and Silvanto, 2022). This observed variability in TMS effects may be attributed to a complex interplay of interindividual differences (e.g., tissue conductivity, gyral shape, E-field direction, and magnitude (Numssen et al., 2023) and the variable response of neuronal networks (Hartwigsen and Silvanto, 2022).

To address individual variability in TMS effects, researchers have turned to biophysical modeling of the induced E-field based on individual head anatomy. This approach has been increasingly used to estimate cortical locations and stimulation strengths at target areas (Van Hoornweder et al., 2022; Nieminen et al., 2015; Thielscher et al., 2015). Common methods that consider the biophysical properties of the head models, along with stimulation parameters like intensity, location, and coil orientation, encompass the boundary element method (BEM; Makarov et al., 2021; Weise et al., 2023) and the finite element method (FEM; Thielscher et al., 2015). These approaches provide realistic estimates of the induced E-field distribution in the head. This allows researchers to explore the effects of different stimulation parameters and optimize TMS protocols for specific brain regions and functions. By correlating the E-field with behavioral or physiological outcome measures, one may identify the neural structures that are effectively stimulated and underlie these effects (Bungert et al., 2017; Laakso et al., 2018; Hartwigsen et al., 2015). In this context, we recently established a novel method to localize the origin of the motor evoked potential (MEP) by combining measurements of hand muscle responses at different coil positions and orientations with simulations of the induced E-field (Weise et al., 2020; Numssen et al., 2021b; Weise et al., 2023). In this so-called “regression approach”, a non-linear (sigmoid-like) correlation between the local E-field and MEP is found at the cortical muscle representation within the primary motor cortex (M1). So far, this powerful

modeling framework has exclusively been used in the primary motor cortex. The current study explored whether and how this approach may be transferred to the cognitive domain in the healthy human brain. We chose attention as a prototypical function that is relevant to all higher cognitive processes and plays a central role in everyday behavior (Johnson and Proctor, 2004; Schuwerk et al., 2017).

With respect to the underlying neural correlates of attention, it has been demonstrated that different attentional subprocesses are organized in various large-scale networks in the human brain (Corbetta and Shulman, 2002). In particular, two separate networks were identified for visuo-spatial attention, related to the voluntary deployment of attention (i.e., attentional orientation) and the reorientation to unexpected events (i.e., attentional reorientation), respectively (Vossel et al., 2014). Attentional orientation is associated with the dorsal attention network (DAN), which comprises the superior parietal lobule (SPL)/intraparietal sulcus (IPS) and the frontal eye fields (FEF) (Szczepanski et al., 2013). In contrast, the ventral attention network (VAN), including the right inferior parietal lobule (rIPL) and the ventral frontal cortex (VFC), is typically involved in detecting unattended stimuli and triggering attentional reorientation (Corbetta et al., 2008). Previous neuroimaging studies have identified the rIPL as a key region for attentional reorientation, and damage to this area can cause severe attention deficits (Igelström and Graziano, 2017; Numssen et al., 2021a). In this study, we applied TMS to the rIPL while participants were performing a Posner-like attentional task (Posner, 1980). We reasoned that direct modulation of task performance with TMS should provide insights into the underlying causal relevance of specific brain regions for a given task (Walsh and Cowey, 2000).

In summary, we first localized attentional processes with functional neuroimaging at the individual subject level and then applied TMS during the attention task over the individually identified rIPL region. Provided that stimulation of well-localized neural populations would be responsible for observed behavioral effects, correlating the individual E-field strength with those effects (i.e., modulations of reaction times) should identify the areas that are effectively stimulated.

Based on previous TMS studies in the domain of attention (Rushworth et al., 2001; Chambers et al., 2004), our main hypothesis was that interfering with rIPL activity during task performance should selectively modulate behavior during attentional reorientation without affecting attentional orientation. We focused on reaction time (RT) modulation to quantify causal effects of the TMS-induced E-fields on attentional processes in a continuous manner. The combination of a behavioral experiment with our previously established localization method should provide new insight into the cortical areas that are relevant for attentional processing. A better understanding of the stimulation effects on cognitive functions will guide more effective stimulation protocols for research and clinical purposes.

As a main result, we only found weak correlations between the cortical stimulation strength and reaction time modulation for the attentional task at the individual subject level. We identified and discussed several factors that potentially impeded larger effect sizes. These limiting factors need to be addressed in future applications of a regression-based TMS localization method to fully leverage its potential for causal brain mapping.

2. Material and methods

We performed a functional magnetic resonance imaging (fMRI) and a TMS experiment to localize the neuronal populations that are responsible for the TMS effect (Figure 1). In the fMRI experiment, we calculated individual activation maps while participants performed the Posner-like task. In the subsequent TMS localization experiment, 500 TMS trials were performed, while the coil was placed at varying positions near the identified activation peak. The regression approach was performed to identify effective targets for attentional reorientation. Cortical locations with the highest correlation between the induced E-field and the behavioral consequences are assumed to be the optimal TMS target for the perturbation of attentional function.

2.1. Participants

Thirty healthy volunteers (15 female, mean age 30.80 ± 5.31 years) were recruited for the fMRI experiment. All participants had normal or corrected to normal vision, and no psychiatric or neurological disorders, or contraindications against TMS or MRI. All participants were right-handed, with a mean laterality index of 90.77 (standard deviation, SD = 10.06) according to the Edinburgh Handedness Inventory (Oldfield, 1971). Written informed consent was obtained from each participant prior to the experiment. The study was approved by the local ethics committee of Leipzig University (ethics number: 371/19-ek). We re-invited seventeen participants (8 female, age 30.12 ± 5.84 years, laterality index 91.24 ± 9.46) to participate in the TMS experiment. Selection criteria were based on fMRI results, with participants being required to show significant activation in the predefined rIPL ROI and a mean error rate in the Posner task below 30%.

2.2. Behavioral task

We used an adapted version of Posner's location-cueing task (Rushworth et al., 2001; Thiel et al., 2004; Numssen et al., 2021a) to trigger orienting and reorienting of spatial attention. The fMRI version of the task contained three trial types: *valid*, *invalid*, and *neutral*, to target different attentional processes (Figure 1). The contrast between invalid and valid trials isolates attentional reorienting processes, and the contrast between valid and neutral trials defines attentional orienting processes/attentional benefits (Grosbras and Paus, 2002; Peelen et al., 2004). During the task, each trial started with the presentation of two rectangular boxes (each size 2.6° of visual angle, with the center situated 8.3° left or right, positioned horizontally) and a fixation cross (size 0.88°) at the center of the screen. To avoid expectancy effects, the duration of fixation (interstimulus interval, ISI) was randomly set to either 2, 3, 4, or 5 s. Subsequently, an arrow was displayed for 250 or 350 ms which served as a cue for the upcoming target location. For valid cues (60 %), the arrow pointed at the side where the target appeared. Participants were trained to orient their attention towards the indicated target position while keeping their fixation at the central fixation cross. For

invalid cues (20 %), the arrow pointed to the opposite side of the target, which required participants to reorient their attention to the target side. Neutral cues (20 %) did not contain any information about the target's location. Finally, a target was presented either at the left or right side (equally distributed) for 2 s. Participants were instructed to identify the positions of the targets by pressing the right/left button using their index and middle fingers as fast and accurately as possible.

We included a total number of 250 trials in the fMRI experiment and 500 in the TMS experiment. The fMRI scan lasted 25 minutes with 150 valid trials, 50 invalid trials, and 50 neutral trials. Participants had a 30 s break in the middle of the task to prevent fatigue (Figure 1a). Before the MRI experiment, participants performed 10 trials as training outside the scanner. In the TMS experiment we specifically focused on attentional reorienting and, thus, only presented valid (75 %) and invalid (25 %) trial types. The ISI was shortened to 3-4 s (Figure 1b). The stimulation lasted approximately 60 min with a short break after every 100 trials. The order of trial types was randomized across participants. Stimuli were administered with Presentation software (v20.1, Neurobehavioral Systems, Berkeley, CA).

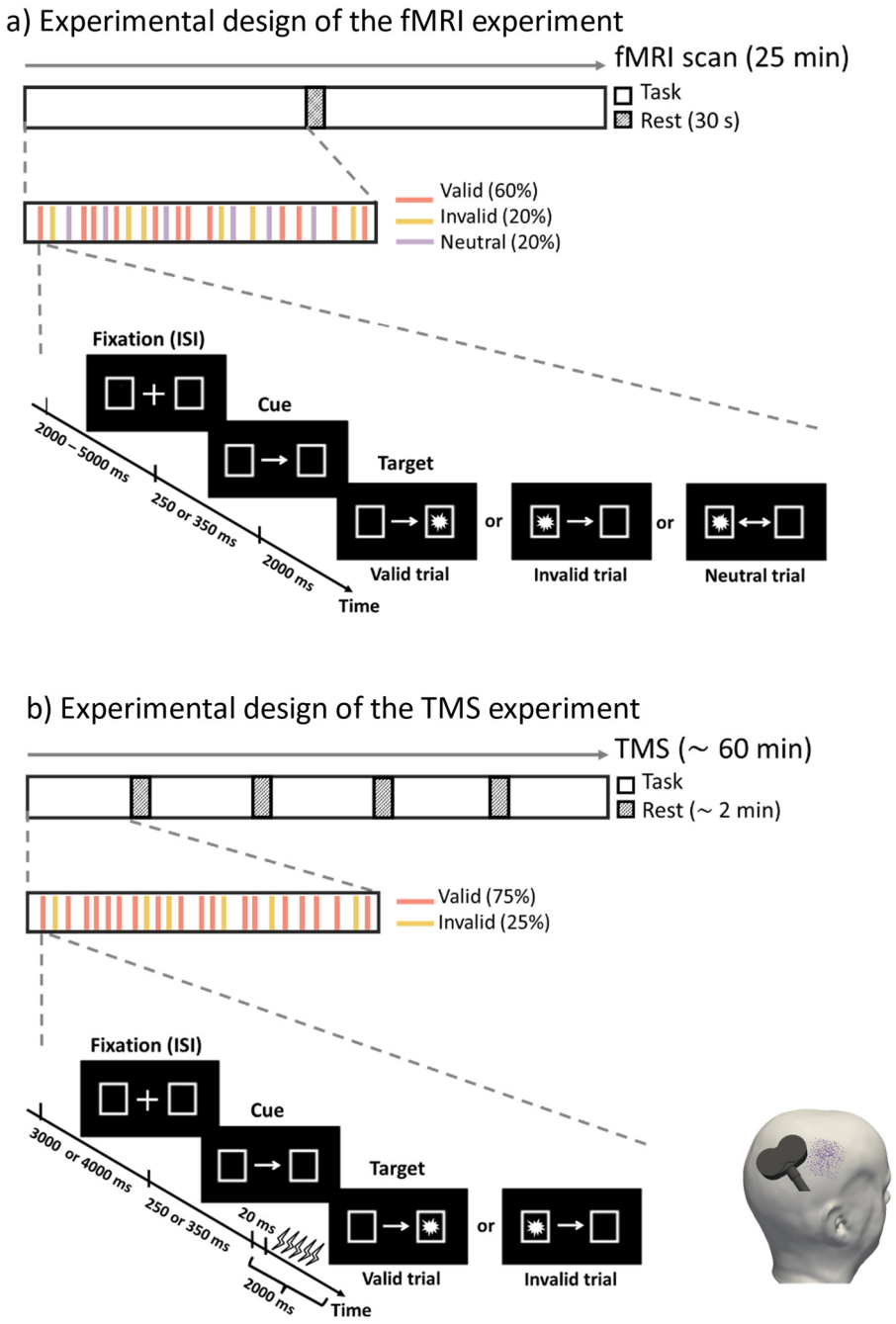

Figure 1. Task paradigm and experimental procedures for the fMRI (a) and TMS experiment (b). A trial consisted of a fixation phase (2-5 s in the fMRI experiment and 3-4 s in the TMS experiment), a cue phase (250 or 350 ms), and a target phase (2 s). Three types of trials (valid, invalid, and neutral) were included in the fMRI experiment, while the neutral condition was excluded in the TMS experiment. A total number of 250 trials were collected in the fMRI experiment. During the TMS experiment, a 5-pulse burst of 10 Hz rTMS was applied 20 ms after the presentation of the target for each trial. 500 TMS trials with random coil positions

(represented by violet dots on the head model) and orientations were collected for further analysis.

2.3. MRI data acquisition

Both functional and structural MRI data were collected using a 3 Tesla Siemens Skyra fit scanner with a 32-channel head coil. To segment the main tissues of the head (scalp, skull, gray matter (GM), white matter (WM), cerebrospinal fluid (CSF), and ventricle) for further calculation of the E-field, T1-weighted, and T2* images were acquired with following parameters: T1 MPRAGE sequence with 176 sagittal slices, matrix size = 256 × 240, voxel size = 1 × 1 × 1 mm^3, flip angle 9°, TR/TE/TI = 2300/2.98/900 ms; T2* with 192 sagittal slices, matrix size = 512 × 512, voxel size = 0.488 × 0.488 × 1 mm^3, flip angle 120°, TR/TE = 5000/394 ms. The T1-weighted image was also used for neuronavigation during TMS. Diffusion MRI with 88 axial slices, matrix size = 128 × 128, voxel size = 1.719 × 1.719 × 1.7 mm^3, TR/TE = 80/6000 ms, flip angle 90°, 67 diffusion directions, b-value 1000 s/mm^3 was acquired for the estimation of the conductivity anisotropy in the WM.

The individual activation map of attentional processing was measured by an event-related fMRI design based on the gradient echo planar (GE-EPI) sequence (60 axial slices, matrix size = 102 × 102, voxel size = 2 × 2 × 2.26 mm^3, flip angle 80°, TR/TE = 2000/24 ms, 775 volumes). Participants were instructed to perform the Posner task that required spatially congruent button presses in response to visual target stimuli.

2.4. MRI data analysis

2.4.1. Preprocessing

MRI data were preprocessed with fMRIPrep 20.1.1 (Esteban et al., 2019), a robust preprocessing pipeline based on Nipype 1.5.0 (Gorgolewski et al., 2011). The individual T1 image was first intensity corrected using N4BiasFieldCorrection (Tustison et al., 2010) and skull-stripped with antsBrainExtraction workflow. Brain tissue segmentation of GM, WM, and CSF was performed on the brain-extracted T1w using FSL FIRST 5.0.9 (Zhang et al., 2001). Brain surfaces were reconstructed using

recon-all from FreeSurfer v6.0.1 (Dale et al., 1999), and the brain mask was refined with a custom variation of the Mindboggle method (Klein et al., 2017) to reconcile ANTs-derived and FreeSurfer-derived segmentations of the cortical gray matter. Volume-based spatial normalization to the MNI152Lin standard space was performed through nonlinear registration with the antsRegistration (ANTs 2.2.0).

Functional data were motion-corrected using mcflirt (FSL 5.0.9) (Jenkinson et al., 2002) and slice-time corrected with 3dTshift from AFNI 20160207 (Cox and Hyde, 1997). Distortion correction was performed by 3dQwarp from the AFNI toolbox. The BOLD time series were then co-registered to the T1w reference using bbregister (FreeSurfer), which implements boundary-based registration (Greve and Fischl, 2009), and resampled into the standard MNI152Lin space by antsApplyTransforms (ANTs). Finally, AFNI 3dmerge was used to spatially smooth the functional data with a 6 mm full-width half-maximum Gaussian kernel.

Several motion-induced confounding regressors were also collected based on the preprocessed BOLD: six corresponding rotation and translation parameters, and framewise displacement (FD) (Power et al., 2014).

2.4.2. Activation analysis

Preprocessed data were analyzed with SPM 12 (Wellcome Department of Imaging Neuroscience, London, UK, http://www.fil.ion.ucl.ac.uk/spm). In the first level analysis, a general linear model (GLM) was generated to estimate task-related neural activities. This consists of three regressors of interest: valid, invalid, neutral, and one regressor of no interest: incorrect or missed responses. These regressors were time-locked to the target onset and modeled with a canonical synthetic hemodynamic response function (HRF) with a duration of 0 s. Additionally, six motion regressors and one volume-masking regressor per FD value above 0.9 (Power et al., 2012) were added to regress out motion-induced artifacts. Trials with RT less than 100 ms or greater than 1000 ms were discarded as incorrect responses (Small et al., 2003). After exclusion, the average number of valid trials remaining for analysis was 145 out of

150 (invalid trials: 47 out of 50; neutral trials: 49 out of 50).

On the second level, two t-contrasts were computed to identify areas preferentially engaged in attentional orienting/benefits (valid vs. neutral trials) and reorienting (invalid vs. valid trials), respectively. The contrast of valid vs. neutral trials isolates brain areas activated in trials with targets appearing at the attended position compared to no spatial expectation. The contrast between invalid and valid trials isolates areas activated by targets appearing at the unattended position after a directional spatial expectation was induced by the cue. False discovery rate (FDR) was used to avoid the bias of multiple comparisons (Benjamini and Hochberg, 1995) with $q < 0.05$. Individual peak activation coordinates of invalid > valid on rIPL were extracted to define the cortical area of interest in the subsequent TMS experiment. The Julich brain atlas (Amunts et al., 2020) was used to define the rIPL mask, which comprises one rostral (PGp) and one caudal (PGa) region in the angular gyrus (AG), and five regions of the supramarginal gyrus (SMG) (PFm, PF, PFop, PGcm, PFt).

2.5. TMS localization experiment

Seventeen of the thirty fMRI participants underwent an online TMS experiment while performing the Posner-like task (Figure 1b). TMS pulses were applied with coil positions over the larger rIPL area using a MagPro X100 stimulator (MagVenture, firmware version 7.1.1) and an MCF-B65 figure-of-eight coil. Coil positioning was guided by a neuronavigation system (TMS Navigator, Localite, Germany, Sankt Augustin; camera: Polaris Spectra, NDI, Canada, Waterloo). The electromyographic (EMG) signal was amplified with a patient amplifier system (D-360, DigitimerLtd., UK, Welwyn Garden City; bandpass filtered from 10 Hz to 2 kHz) and recorded with an acquisition interface (Power1401 MK-II, CED Ltd., UK, Cambridge, 4 kHz sampling rate) and Signal (CED Ltd., version 4.11).

To determine the optimal stimulation intensity, we manually measured the resting motor threshold (rMT) of the participants' right index fingers with one surface electrode positioned over the first dorsal interosseous (FDI) muscle belly and one at

the proximal interphalangeal joint (PIP). During the rMT measurement, we first positioned the TMS coil over the left-hand knob, which was identified based on established anatomical landmarks (e.g., Diekhoff et al., 2011). The coil was initially placed at 45° to the midline, and then moved around until the optimal coil location and orientation were identified based on the MEP response. The rMT was defined as the minimum stimulator intensity to induce an MEP larger than 50 μV in at least 5 of 10 consecutive trials (Beynel et al., 2019).

500 bursts of rTMS with 5 pulses at 10 Hz each were applied at 100% rMT (Rushworth et al., 2001) during the 500 Posner-like task trials, comprising 375 *valid* trials (75%) and 125 *invalid* trials (25%). The bursts were initiated 20 ms after the target presentation to disrupt attentional processing transiently (Figure 1b). After every 100 trials, a short break of ~2 min was advised to avoid fatigue. We restricted the area over which the coil centers were located to a circular zone of 3 cm radius around the individual fMRI-derived activation peak (invalid > valid trials) in the rIPL. Stimulation area centers were moved 2 cm anterior/superior in 4 subjects because their activation peaks were close to the occipital or temporal lobe. Coil positions and orientations were randomly selected within the defined circular zone for each burst, to increase electric field variability by minimizing cross-correlations between induced electric fields (Numssen et al., 2021b). The range of coil orientations was limited to 60° (± 30° from the traditional 45° orientation) due to hardware constraints such as the spatial restriction of the navigation system and the obstruction of the coil handle and cable. Note that eleven participants were sampled with a "quadrant mode": we randomly sampled 100 stimulations for each quadrant of the stimulation area, resulting in 400 trials. The final 100 trials were arbitrarily attributed across the whole stimulation area. To diminish possible sequential effects, we used a "random mode" for the remaining six participants: all 500 trials were randomly sampled throughout the experimental session. Coil positions and corresponding behavioral responses, i.e., reaction time and accuracy, were recorded for each trial.

2.6. TMS mapping

2.6.1. Numerical simulations of the induced electric field

Individual head models were reconstructed using the headreco pipeline (Nielsen et al., 2018) utilizing SPM12 and CAT12 (http://www.neuro.uni-jena.de/cat/) for all seventeen subjects. The final head models were composed of approximately 3.4×10^6 nodes and 20×10^6 tetrahedra (average volume: approximately 0.15 mm^3 in the cortex). Seven tissue types were included with standard conductivity estimates: white matter (σ_{WM} = 0.126 S/m), gray matter (σ_{GM} = 0.275 S/m), cerebrospinal fluid (σ_{CSF} = 1.654 S/m), bone (σ_B = 0.01 S/m), skin (σ_S = 0. 465 S/m), ventricle (σ_V = 1.654 S/m) and eyeballs (σ_{EB} = 0.5 S/m) (Thielscher et al., 2015; Wagner et al., 2004). WM and GM were assigned anisotropic conductivities while the five other tissues were treated as isotropic. Electric fields induced by coil positions of all TMS trials were then computed considering individual head geometry and employing the FEM-based solver implemented in SimNIBS v3.2.6 (Saturnino et al., 2019; Thielscher et al., 2015). See Saturnino et al. (2019) for more details on the numerical simulation.

A refined region of interest (ROI) was defined around the rIPL area based on the Julich brain atlas (Amunts et al., 2020) to improve the numerical resolution around the selected ROI. All analyses were performed on the mid-layer between GM and WM surfaces to avoid boundary effects of the E-field due to conductivity discontinuities.

2.6.2. Regression analysis

The regression approach used in this study is based on a recently developed modeling framework in the motor cortex (Weise et al., 2020; Numssen et al., 2021b; Weise et al., 2023). The principal idea of the regression approach is to combine the outcome of multiple stimulation experiments with the induced E-fields of different coil positions and orientations, assuming that, at the effective site, the relationship between E-field and behavioral performance is stable, i.e., the same electric field strength always evokes the same behavioral output. In particular, the method leverages more

information by simultaneously varying both coil positions and orientations exploiting electric field variability to avoid bias towards locations with high E-field magnitudes, such as the gyral crown.

We first discarded TMS trials with RT $<$ 100 ms or RT $>$ 1000 ms, and those with a coil distance $\geq$ 5 mm from the skin surface. After applying these exclusion criteria, the average number of trials remaining for analysis was 115 (out of 125) for the invalid condition, and 365 (out of 375) for the valid condition. Subsequently, the valid trials were randomly downsampled to match the number of invalid trials to guard against potential sample-size-dependent effects. In addition, any linear trends of RT over time were removed to mitigate potential learning or fatigue effects.

After data cleaning, we performed Linear regression analysis to identify the neural populations that are causally involved in attentional processing for every element within the ROI (Weise et al., 2020). The linear relationship between E-field magnitude $x_{i,j}$ of TMS trial i ($1 \leq i \leq N_{TMS}$) at the cortical element j ($1 \leq j \leq N_{elms}$) and the estimated RT $\hat{y}_{i,j}$ is calculated:

$$\hat{y}_{i,j} = \alpha_j + \beta_j x_{i,j}$$

Here, α is the intercept and β is the slope. We set the constraint of α and β to (-3000, 3000) and (-1000, 1000), respectively.

The site of effective stimulation can be quantified by the goodness-of-fit (GOF), which would be highest at the cortical site that houses the relevant neuronal populations (Numssen et al., 2021b). We assessed the element-wise GOF by the coefficient of determination R^2:

$$R_j^2 = 1 - \frac{VAR\ (y\ -\ \hat{y}_j)}{VAR\ (y)}$$

where y is the measured RT, and $\hat{y}_j$ is the estimated RT. The R^2 value measures how well the regression model explains the observed data, with higher R^2 denoting better fitting results.

The regression analysis was applied separately to invalid and valid trials and yielded

one R^2 score each for valid and invalid conditions per ROI element. We replaced all negative R^2 values with 0, as these denote numerical errors and are very small. To assess the significance of the observed R^2 values and determine if they could be explained by chance alone, we randomly shuffled the RT values 1000 times and performed the linear regression analysis for each permutation. Only R^2 values that exceeded the 5th percentile of the shuffled data were deemed statistically significant.

We then multiplied the raw R^2 value with the slope's sign to include not only the goodness of fit (R^2) but also the direction of the TMS effect in one metric:

$$\tilde{R}_j^2 = R_j^2 \cdot \text{sign}\,(\beta_j)$$

This allowed us to visually differentiate cortical areas of inhibitory TMS effects (positive slope areas) from areas of facilitatory TMS effects (negative slope areas). We assumed that high-frequency rTMS on rIPL will selectively impair performance on invalid trials, resulting in higher $\tilde{R}_j^2$ values compared to valid trials.

To generate the group $\tilde{R}^2$ map, all individual $\tilde{R}^2$ maps were first mapped to the group averaged brain template, then voxel-wise $\tilde{R}^2$ values were averaged across subjects.

3. Results

3.1. Behavioral performance

Behavioral results from the fMRI experiment showed a reliable difference of RT between conditions ($F_{2,87}$ = 5.38, p < 0.01; invalid$_{fMRI}$: 403 ± 69 ms; valid$_{fMRI}$: 345 ± 70 ms; neutral$_{fMRI}$: 384 ± 72 ms). Post-hoc t-tests confirmed a reorienting effect, that is, slower RTs for invalid compared to valid targets (t_{29} = 15.25, p < 0.01). There was no significant difference between neutral and valid or invalid trials (Figure 2a). No significant differences were found in accuracy ($F_{2,87}$ = 0.92, p = 0.40; invalid$_{fMRI}$: 0.95 ± 0.08, valid$_{fMRI}$: 0.97 ± 0.06, neutral$_{fMRI}$: 0.95 ± 0.06).

In the TMS experiment, we again found a significantly slower response speed for invalid relative to valid trials (t_{16} = 12.76, p < 0.01; invalid$_{TMS}$: 357 ± 62 ms; valid$_{TMS}$:

286 ± 61 ms). In line with our hypothesis, task accuracy was also significantly decreased in the invalid condition (t_{16} = 4.16, p < 0.01; invalid$_{TMS}$: 0.93 ± 0.06; valid$_{TMS}$: 0.99 ± 0.02) (Figure 2b).

Note that subjects had generally faster RTs in the TMS experiment compared to the fMRI session. These behavioral differences between sessions inside and outside of the MRI scanner might be driven by unspecific distracting factors inside the scanner, such as the supine position and the noise, which could slow down motor execution times and decrease attentional focus inside the MRI scanner (Jamadar et al., 2010; van Maanen et al., 2016; Koch et al., 2003).

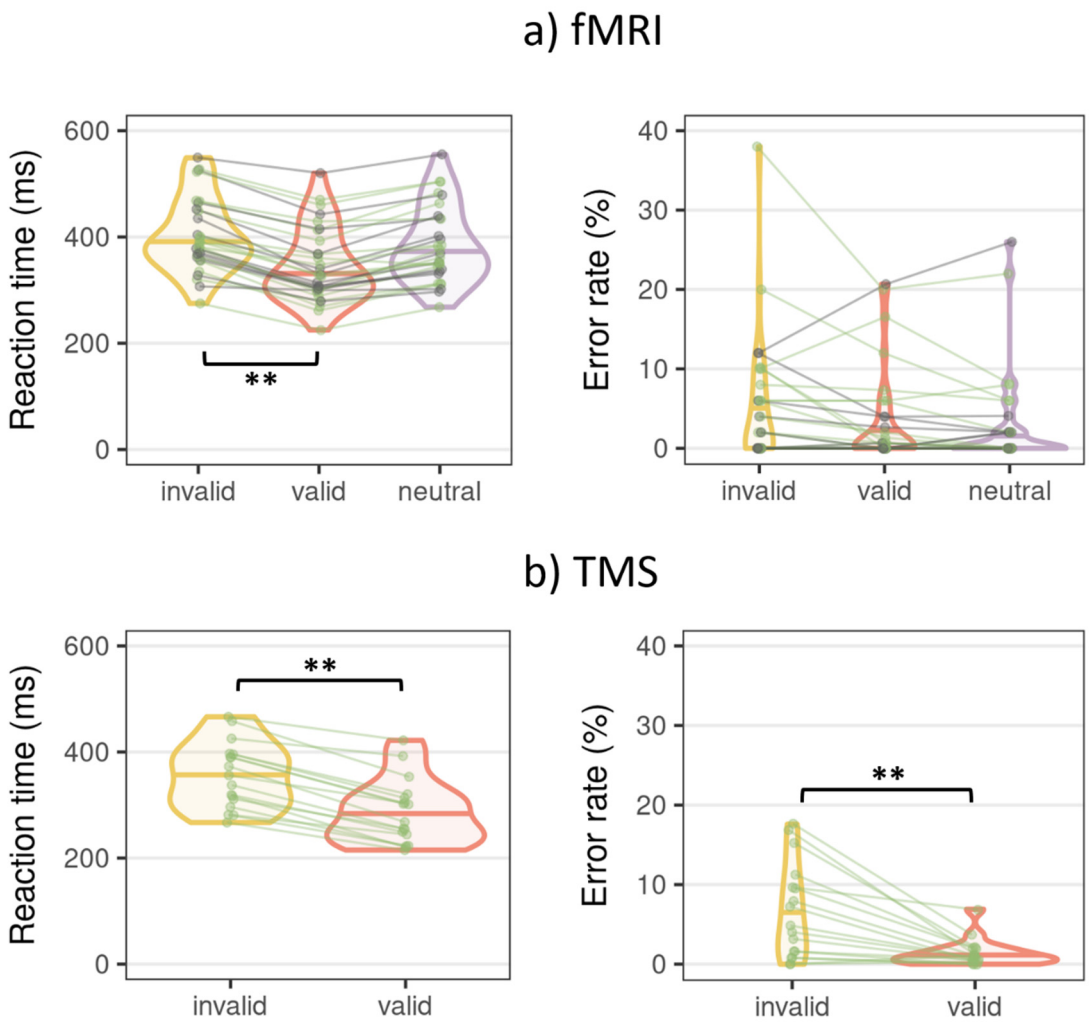

Figure 2. Behavioral results of the Posner task during fMRI and TMS. Reorienting attention (*invalid* trials) was significantly slower than attentional orientation (*valid* trials), both in the

fMRI (a) and in the TMS (b) realization. For task accuracy, significant differences were only present during TMS. ** $p < 0.01$. Green points/lines: subjects who participated in both fMRI and TMS sessions; grey points/lines: subjects who only participated in the fMRI experiment.

3.2. fMRI activation

The fMRI results revealed distributed bilateral brain regions from different networks for the reorienting of attention (Figure 3a). These include the ventral attention network (IPL, MFG), the dorsal attention network (SPL, FEF), and the salience network (Insula; anterior cingulate cortex, ACC). In contrast, the default mode network (DMN) (posterior cingulate cortex, PCC; medial prefrontal cortex, mPFC) was deactivated for invalid relative to valid trials. These findings go beyond the classic view of a ventral, right-lateralized reorientation system. Relative to the neutral condition, attentional orienting showed deactivation of both IPS and SPL, but increased activation of mPFC (Figure 3b). All activations are reported at the level of $q < 0.05$ after FDR correction.

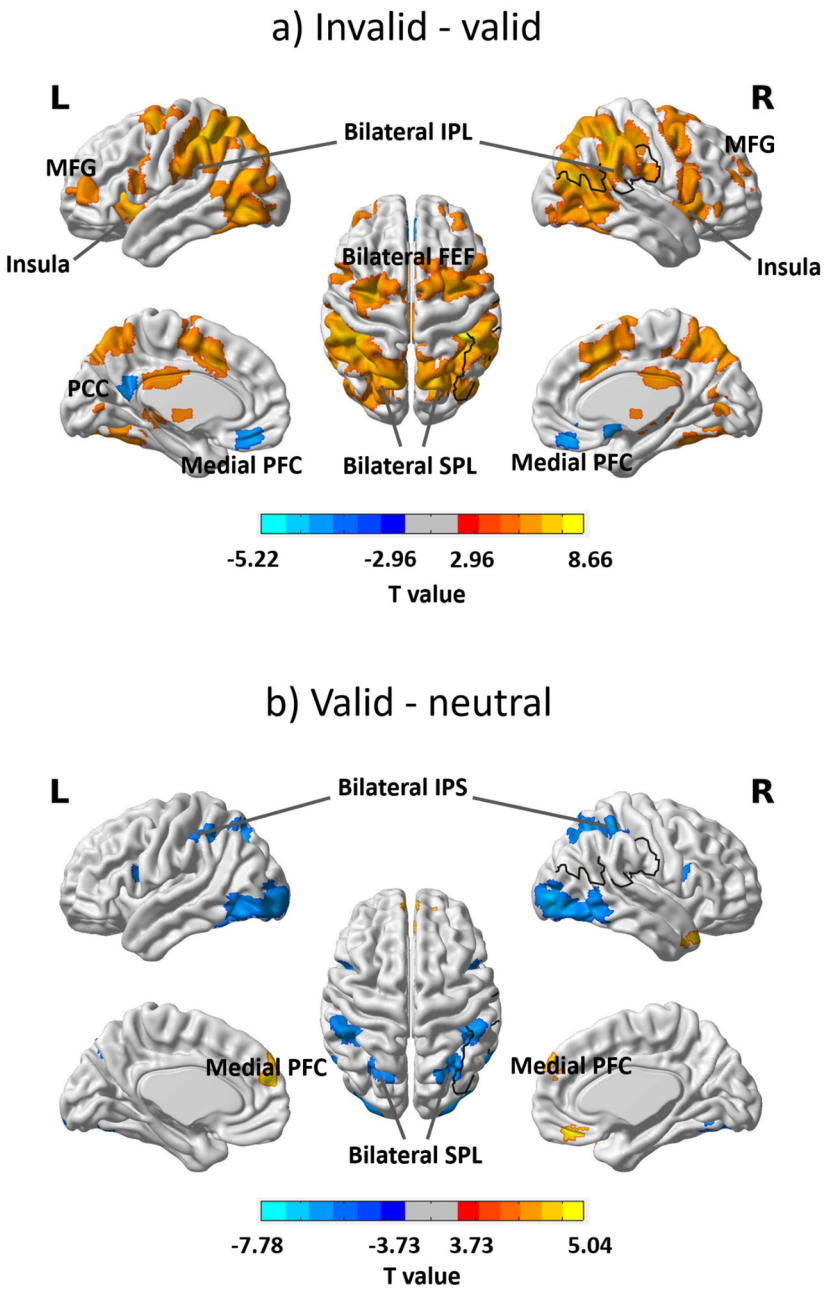

Figure 3. Spatial attention recruits distributed networks: fMRI activation results during attentional orientation and reorientation. (a) Relative to valid trials, the invalid condition exhibits significant activation in both the dorsal and ventral attention networks, as well as the salience network. (b) Attentional orientation resulted in increased activation of the medial prefrontal cortex and deactivation of parietal areas (FDR correction, $q < 0.05$).

3.3. TMS mapping results

At the group level, the relationship between the induced E-field and the behavioral modulation differed significantly between valid and invalid trial types (Figure 4). Specifically, the group-level $\tilde{R}^2$ maps for the invalid condition were dominated by positive correlations, i.e., higher E-field leads to a slower response, implying a perturbation effect on the invalid condition. On the contrary, the group-level $\tilde{R}^2$ map for the valid condition was close to zero indicating that there was no effect of TMS for attentional orientation (Figure 5).

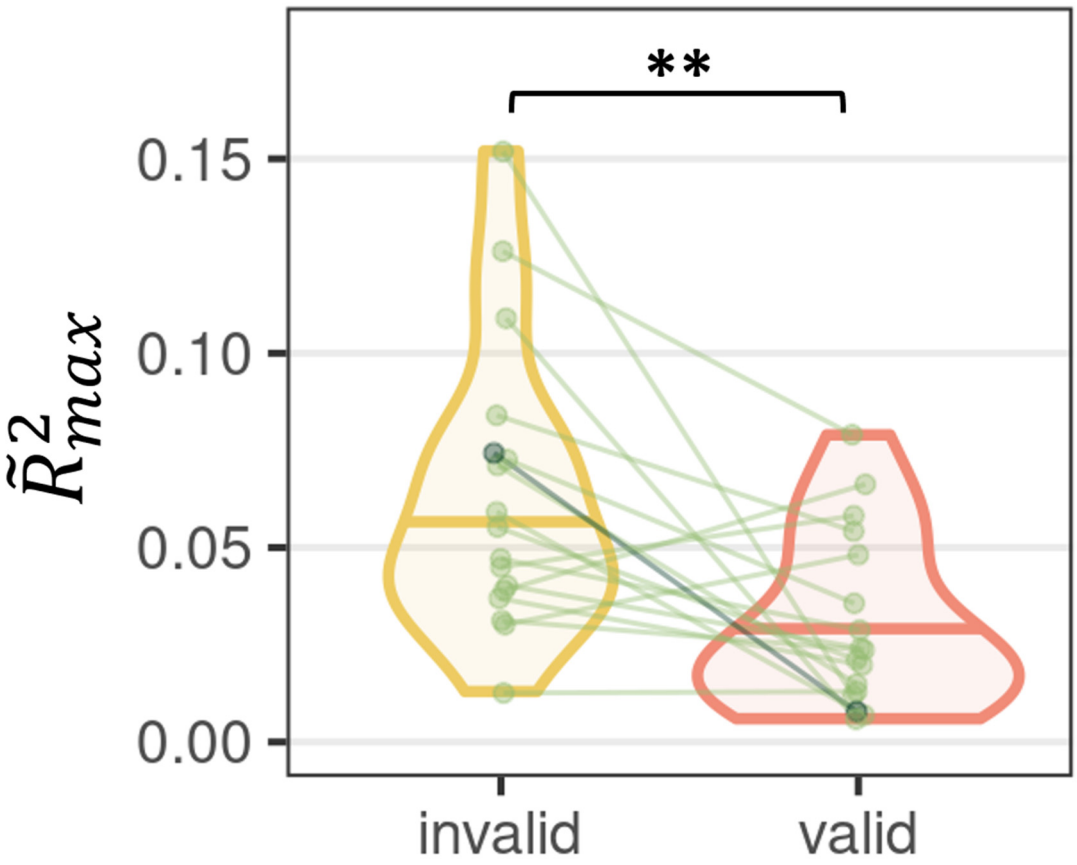

Figure 4. TMS selectively affects attentional reorienting. Invalid trials (reflecting attentional reorienting) were significantly stronger related to the induced E-field than valid trials (reflecting attentional orientation). *: $p < 0.05$. Green points/lines: single subjects. The dark green points/line indicate subject-14, whose detailed $\tilde{R}^2$ results are shown in Figure 6.

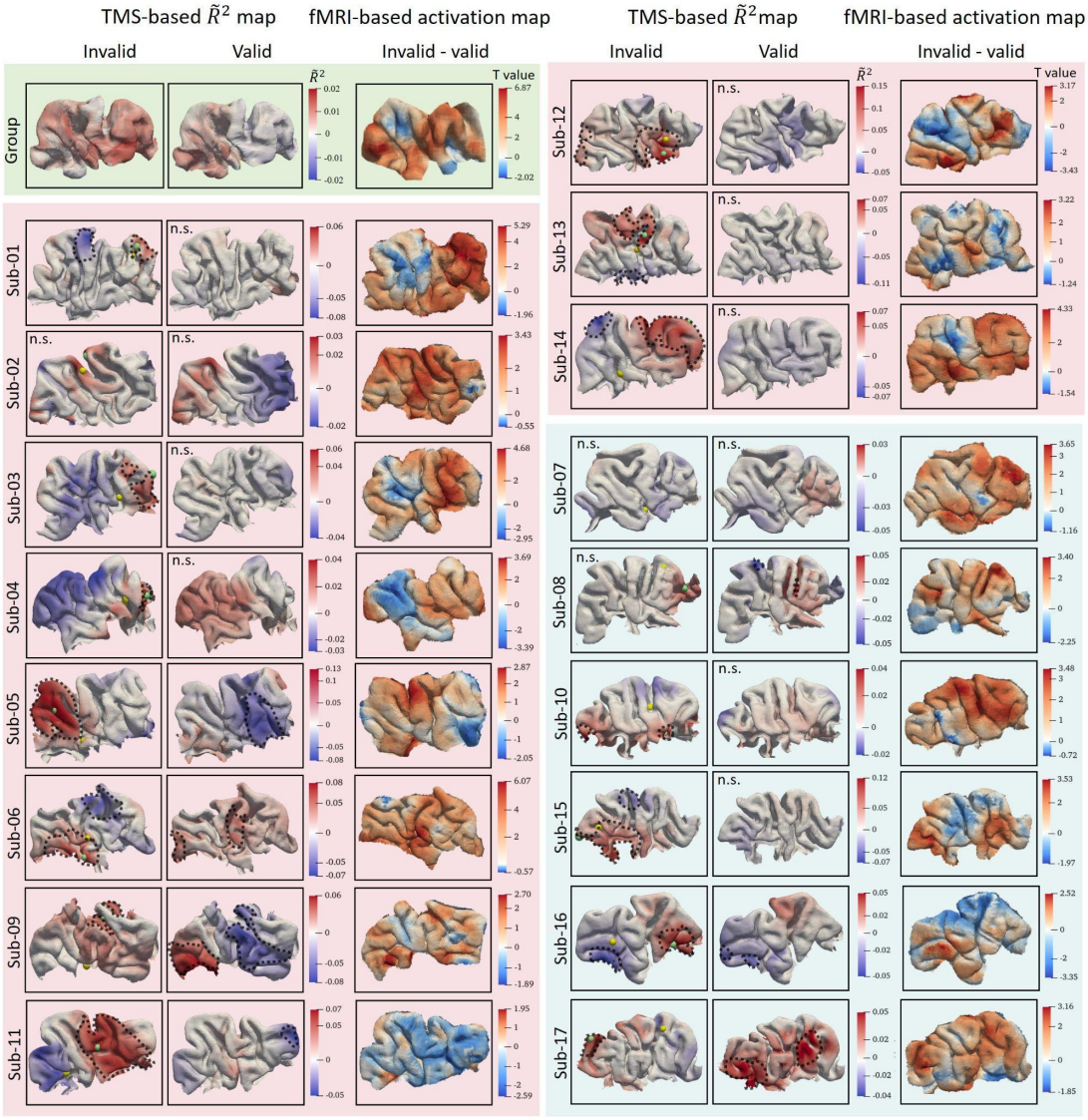

Figure 5. Inhibitory TMS effects on attentional reorientation are subject-specific. This figure shows the group (green background) and individual $\tilde{R}^2$ maps (pink and cyan background) on the rIPL, as well as the corresponding activation maps. $\tilde{R}^2$ maps were generated by R^2 scores multiplied with the slope's sign to represent the direction information of the linear correlation. Pink background color codes subjects sampled with "quadrant mode", while cyan color denotes "random sampling mode" (see text). Yellow spheres in the invalid column represent the fMRI activation peak location of the invalid-valid contrast, whereas green spheres denote the peak $\tilde{R}^2$. The black contours marked the brain areas that showed significant R^2 values after the permutation test. Note that the $\tilde{R}^2$ scores were mapped onto the mid-layer surface between white and grey matter whereas the fMRI activation results are mapped onto the

cortical grey matter surface. N.s.: not significant.

In Figure 6, we present results for a representative subject with moderate fitting results to show the linear regression maps from prominent locations. As shown at three elements (one with the highest GOF of negative linear trend, one on the activation peak, and one with the highest GOF of positive linear trend), the correlation between measured RTs and the computed E-fields did not show a clear S-shaped curve, as MEP data did (Weise et al., 2020; Numssen et al., 2021b).

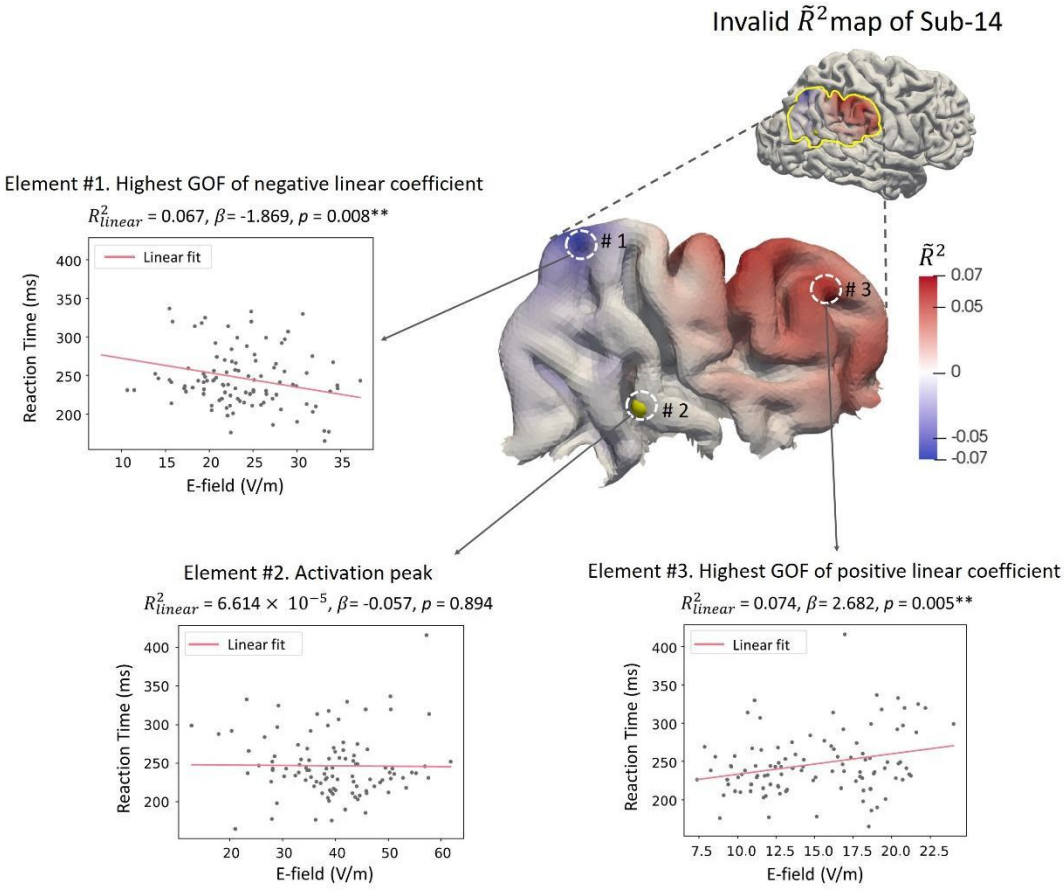

Figure 6. TMS-induced modulation of attentional reorientation from one representative subject with moderate GOF (sub-14). The $\tilde{R}^2$ map is derived from voxel-wise linear regression of invalid trials, multiplied with the sign of slope to include information about

inhibitory (positive slope values) versus facilitatory TMS effects (negative TMS values). The linear fitting lines are shown for 3 elements: #1 with the highest GOF of negative linear correlation, #2 is the fMRI activation peak of reorientation, and #3 with the highest GOF of positive linear correlation. The yellow sphere embedded in the gyral crown marks the location of the fMRI activation peak. β denotes the slope of linear regression, and p values are the significant level of β. **: $p < 0.01$. Grey points: single TMS trials.

Figure 5 displays the results of the TMS and fMRI studies, both at the group and single-subject level, for all seventeen participants. The green background shows the group-averaged results, while the pink and cyan backgrounds represent the "quadrant sampling mode" and "random sampling mode", respectively. The black contours on the R^2 maps mark brain areas showing significant R^2 values after the permutation test. On the subject level, the $\tilde{R}^2$ maps exhibit considerable individual variability, indicating distinct and subject-specific patterns of TMS modulatory effects on spatial attention. Furthermore, the comparison between fMRI activation maps and TMS-based $\tilde{R}^2$ results identified differences in BOLD-measured neuronal activity and TMS-evoked neuronal effects. In the group-averaged $\tilde{R}^2$ maps, we observed a weak positive correlation in the rIPL cortical region during the invalid condition, indicating a delayed response speed with increased E-field exposure. However, the pattern for the valid condition is less definitive.

In terms of the magnitude of $\tilde{R}^2$, Table 1 shows the individual maximum $\tilde{R}^2$ scores for the invalid and valid conditions. Given that the TMS revealed an inhibitory effect on attentional processing, we only presented $\tilde{R}^2$ scores that show a positive correlation between E-field and RT in Table 1. A Wilcoxon signed rank test revealed a significant difference of the maximum $\tilde{R}^2$ between the two conditions ($Z = 2.979$, $p < 0.01$; $\tilde{R}^2_{invalid} = 0.064 \pm 0.037$, $\tilde{R}^2_{valid} = 0.031 \pm 0.022$) (Figure 4). Compared with the valid condition, the $\tilde{R}^2$ values are higher in the invalid condition, identifying a stronger disruptive effect of the E-field on the response speed during attentional reorienting.

Table 1. Individual activation peaks and TMS results.

Subject ID	Activation peak	MT	Invalid $\tilde{R}^2_{max}$	Valid $\tilde{R}^2_{max}$
01	(56, -37, 34)	43%	0.055	0.021
02	(42, -55, 50)	39%	0.031	0.024
03	(60, -41, 31)	70%	0.059	0.007
04	(54, -33, 34)	47%	0.041	0.024
05	(54, -61, 18)	57%	0.127	0.079
06	(62, -57, 34)	64%	0.084	0.054
07	(52, -53, 16)	46%	0.013	0.013
08	(42, -73, 40)	43%	0.030	0.048
09	(56, -63, 25)	45%	0.039	0.066
10	(58, -47, 36)	45%	0.037	0.02
11	(46, -69, 20)	42%	0.073	0.036
12	(69, -39, 34)	53%	0.152	0.012
13	(52, -51, 31)	56%	0.071	0.015
14	(54, -67, 27)	38%	0.074	0.008
15	(42, -77, 29)	40%	0.109	0.006
16	(56, -67, 34)	52%	0.047	0.029
17	(58, -47, 50)	44%	0.045	0.058
Group average	(51, -55, 32)	48%	0.064	0.031

Notes: The Activation peak column provides individual fMRI peak coordinates in the rIPL for the invalid-valid contrast in standard MNI space. The individual resting motor threshold (MT) is provided in the percentage of maximum stimulator output (% MSO), and the maximum $\tilde{R}^2$, both for invalid and valid conditions with positive correlations between E-field and RT.

4. Discussion

We applied our previously established regression approach to localize the neuronal underpinnings of attentional processes with TMS. In this statistical approach, cortical stimulation exposure across multiple stimulation sites is related to the TMS-induced change in behavior. Here, we studied the relation between the strength of the TMS-

induced E-field in the cortex and the inhibitory effects of TMS on spatial attention, to identify relevant cortical regions for attentional processing within the rIPL. We found a weak correlation between E-field strength and attentional performance, highlighting that the translation of the regression approach from motor function to cognitive domains is challenging. On the group level, we observed that the task-specific inhibitory TMS effect was more profound on attentional reorienting, compared to attentional orienting. On the single-subject level, the regression analyses identified large individual variability, both for the cortical organization as well as for TMS responsiveness. In addition, we identified differences in BOLD-measured neuronal activity and TMS-evoked neuronal effects. This incongruence highlights the principal distinction between neural activity being correlated with (or maybe even caused by) particular paradigms, and activity of neural populations exercising a causal influence on the behavioral outcome.

4.1. fMRI results

The ability to orient attention is a fundamental component of most perceptual-motor processes in everyday life (Natale et al., 2009). Consequently, we took our first step in generalizing the regression method to spatial attention. Spatial orienting can be driven either endogenously, by predictive contingencies, i.e., top-down cues, or exogenously, by unexpected bottom-up signals stemming for example from visual inputs. These processes are accomplished by the interaction of several cortical regions, forming functional networks (Chica et al., 2011). Our fMRI results show that large-scale brain networks were activated during attentional reorienting, including both dorsal and ventral attention networks, which reflects the neural bases of the interplay between these two attention mechanisms (Shulman et al., 2009; Proskovec et al., 2018). One of these regions, the rIPL, is consistently identified as a major network hub in diverse cognitive functions, from bottom-up perception to higher cognitive capacities that are unique for humans (Cabeza et al., 2012; Igelström and Graziano, 2017).

The rIPL is a large region that comprises two major gyri: SMG and AG, separated by the intermediate sulcus of Jensen (Segal and Petrides, 2012). Previous studies

suggested that both SMG and AG are critical for attention shifts between visual stimuli (Chambers et al., 2004). A behavioral and functional connectivity-based meta-analysis study further defined the functional topography of rIPL (Wang et al., 2016). This study revealed that the SMG primarily participates in attention, execution, and action inhibition, while the AG is involved in social and spatial cognition. In line with our group activation results, both SMG and AG exhibited significant activation during attentional reorientation, supporting their involvement in basic attention and spatial cognition.

It is worth noting that we found bilateral IPL and VFC activated when participants attempted to process the target at an unexpected location, which challenges the traditional view that the VAN is lateralized to the right hemisphere (Lunven and Bartolomeo, 2017). The comparison of attentional orientation and neutral trials (valid - neutral) allowed us to separate attentional benefits from visual, motor, or other basic cognitive tasks (i.e., valid - baseline), and to explore the influence of cue predictiveness on spatial attention. Previous studies could not provide conclusive explanations for this effect of top-down predictions. Some researchers observed significant activation for valid minus neutral trials in either DAN or VAN (Peelen et al., 2004; Natale et al., 2009), while others found a significant deactivation of the rIPL when participants are orienting their attention to the predictive cues (Doricchi et al., 2010). Our results demonstrate that, when attention was focused on the valid side, bilateral IPS and SPL were suppressed, potentially to prevent reorienting to distracting events. Specifically, activation of medial PFC as a part of DMN may indicate an endogenous focus. These findings provide new insight into the functional contribution of the brain regions involved in spatial attention.

4.2. TMS localization

We performed state-of-the-art FEM-based E-field simulations to allow for realistic quantifications of the effect of cortical stimulation on attentional processes. At the group level, TMS led to an interference effect on attentional processing, which is in line with our hypothesis that TMS on rIPL should selectively perturb the reorientation

of attention (Rushworth et al., 2001). This specificity of the TMS effect is reflected in significantly stronger relationships between E-field exposure and behavioral modulation for attentional reorientation, as compared to attentional orientation. In general, the TMS-induced effect, measured by the coefficient of determination $\tilde{R}^2$, was much lower for attention as compared to the motor domain, in which the TMS regression approach was previously established (Weise et al., 2020; Numssen et al., 2021b). Lower $\tilde{R}^2$ values likely reflect the more restricted impact of the E-field on reaction time compared to its effect on muscle recruitment when stimulating the primary motor cortex.

In fact, TMS studies with cognitive paradigms often show high inter-individual variability and results are not always conclusive (Bergmann and Hartwigsen, 2021). Moreover, some cognitive paradigms suffer from relatively low test-retest reliability which may contribute to the strong variability of behavioral results (Hedge et al., 2018). The key problem is that the underlying neural basis of cognitive functions is much more complex and variable than that of eliciting hand muscle twitches (Fetsch, 2016). In our study, in spite of this high variability, we were still able to distill out the TMS effect on attentional reorienting. However, the large amount of residual variance indicates that taking into account additional variables and more complex models (e.g., multivariate regression) is likely to improve accuracy and reliability.

4.3. TMS vs. fMRI localization

We paralleled the fMRI-based activation maps with TMS-based cortical mapping to explore the gains of regression-based functional TMS mappings in the domain of spatial attention. Our behavioral results suggest that rTMS over the rIPL impaired attentional reorientation, leading to increased response latencies and potentially decreased task accuracy.

The comparison between BOLD-measured neuronal activity obtained from fMRI and neuronal stimulation effects evoked by TMS revealed notable discrepancies. This incongruence highlights the principal distinction between neural activity being

correlated with or potentially caused by particular paradigms and the activity of neural populations that exert a direct causal influence on the behavioral outcomes. While fMRI provides information about overall neural responses associated with spatial attention, TMS offers insights into the specific and causal effects of targeted neural modulation.

4.4. Transferring the TMS regression approach to the study of cognition

The TMS regression approach integrates information from multiple stimulation patterns to map structure-function relationships based on the causal effect of the induced electric field. The main metric to separate cortical locations is the explained variance of the behavioral modulation ($\tilde{R}^2$). However, when applied to attentional processes, the explained variance is relatively low. In comparison to the motor domain, where up to 80% of the variance can be explained at the single subject level (Numssen et al., 2021b), only 10% of the individual variance could be explained in the attention domain in the present study. These comparatively low $\tilde{R}^2$ values for attentional processes probably stem from various sources.

As a first potential explanation for the observed discrepancy between the motor and attention domains, behavioral responses to cognitive tasks intrinsically exert higher variance due to complex processing demands (Hedge et al., 2018) that give rise to confounding factors, such as fatigue or differences in the mental state. Additionally, the organization of the rIPL is challenging to study due to the complex anatomy and highly divergent functional segregation of this cortical region (Williams et al., 2022; Krall et al., 2016).

Another potential factor that may affect the explained variance is the spread of attentional task processing across the cortex. In contrast to the focal representations within the motor system, a multitude of cortical locations may interact with the stimulation effect during attentional processing. The TMS trials with different coil positions/orientations may differentially target cortical sites that have various

functions. Some of the varying targets can accumulate and thus exert inhibitory or excitatory effects, others might neutralize the TMS effect. Previous studies confirmed that compared to single-node TMS, concurrent frontal-parietal network TMS showed a reduction of the reorienting effect in the right hemifield (Gallotto et al., 2022). Therefore, network effects should be considered in future studies. One possibility would be the multivariate regression schemes.

Several limitations may have contributed to the limited explained variance. Firstly, we did not adjust the stimulation strength to account for the differences of the cortical depths between the primary motor cortex, where the rMT was assessed, and IPL, where the regression localization approach was performed. Instead, we used the same intensity of 100% rMT as in previous studies (Rushworth et al., 2001) to modulate spatial attention. Ignoring potential individual differences between brain regions may have contributed to the observed variability of the current study. To elaborate on this potential shortcoming, we further computed E-field ratios between the rIPL and the M1 hotspot for all participants. This revealed that the E-field exposure in the rIPL was consistently lower (maximum ratio = 0.95, minimum ratio = 0.25, median ratio = 0.73 across subjects). Subsequently, we conducted Spearman correlation analyses to explore the relationship between the E-field ratio and the maximum $\tilde{R}^2$ value across participants to further explore if stronger stimulation yielded better functional localization. However, the results did not reach statistical significance ($\rho_{invalid}$ = 0.18, p = 0.48).

Secondly, the current study employed the 5/10 methods to determine the rMT, which is defined as the minimum stimulus intensity required to elicit a peak-to-peak MEP amplitude greater than 50 μV in 5 out of 10 consecutive trials. This rMT determination method has been reported as relatively less reliable than the 10/20 method, which requires eliciting an MEP amplitude greater than 50 μV in 10 out of 20 consecutive trials (Awiszus, 2012). Therefore, the utilization of the 5/10 method could potentially contribute to additional sources of variance. In addition, while we attempted to maximize the range of coil orientations to minimize potential cross-

correlations between electric fields, hardware limitations, such as the visible range of positions in the navigation system and coil handle obstruction, limited the true orientation range to 60°.

Finally, it should be noted that the interaction between internal factors such as the current brain state, fatigue, baseline performance level, and external stimulation parameters such as intensity, frequency, and duration is not well understood (Hartwigsen and Silvanto, 2022). Such interactions may induce strong inter-individual variability in response to TMS in studies of cognition. Nonetheless, transferring the TMS regression approach to cognitive domains is promising and will ultimately help to optimize TMS protocols for a wide range of applications. Future work should explore network effects of different TMS protocols, dosing, and individual differences in response to TMS.

5. Conclusion

To conclude, we applied a localization approach based on functional analyses of the TMS-induced E-fields and their behavioral modulation in a cognitive domain. With this causal approach, we quantified TMS effects on attentional reorientation and highlighted, both, interindividual variation in cortical organization and differences between fMRI activity and TMS mapping. The results show that E-field modeling can play a valuable role when exploring structure-function relationships with non-invasive brain stimulation methods. We are confident that our approach of combining E-field modeling and behavioral modulation can be further generalized and applied to other functional domains to increase TMS effectiveness and allow its applications at the individual level. To increase the specificity and sensitivity of the method, we suggest developing multivariate regression approaches that account for the recruitment of distributed networks for different cognitive functions. Moreover, alternative readout variables, such as physiological (e.g., heart rate) and electrophysiological (e.g., TMS-evoked electroencephalogram potentials) measures may further increase the information obtained from TMS mapping in cognitive studies.

Acknowledgments

The authors would like to acknowledge the support from the German Research Foundation (grant no. HA 2899/31-1, HA 6314/9-1, KN 588/10-1 to JH, GH and TRK; and grant no. WE 59851/2 to KW). GH is supported by the Max Planck Society and the European Research Council (ERC-2021-COG 101043747). YJ would also like to thank the China Scholarship Council for its financial support.

Declaration of interests

The authors declare no competing interests.

References

AMUNTS, K., MOHLBERG, H., BLUDAU, S. & ZILLES, K. 2020. Julich-Brain: A 3D probabilistic atlas of the human brain's cytoarchitecture. *Science,* 369**,** 988-992.

AWISZUS, F. 2012. On relative frequency estimation of transcranial magnetic stimulation motor threshold. *Clinical neurophysiology: official journal of the International Federation of Clinical Neurophysiology,* 123**,** 2319-2320.

BENJAMINI, Y. & HOCHBERG, Y. 1995. Controlling the false discovery rate: a practical and powerful approach to multiple testing. *Journal of the Royal statistical society: series B,* 57**,** 289-300.

BERGMANN, T. O. & HARTWIGSEN, G. 2021. Inferring causality from noninvasive brain stimulation in cognitive neuroscience. *Journal of cognitive neuroscience,* 33**,** 195-225.

BESTMANN, S. & FEREDOES, E. 2013. Combined neurostimulation and neuroimaging in cognitive neuroscience: past, present, and future. *Annals of the New York Academy of Sciences,* 1296**,** 11-30.

BEYNEL, L., APPELBAUM, L. G., LUBER, B., CROWELL, C. A., HILBIG, S. A., LIM, W., NGUYEN, D., CHRAPLIWY, N. A., DAVIS, S. W. & CABEZA,

R. 2019. Effects of online repetitive transcranial magnetic stimulation (rTMS) on cognitive processing: a meta-analysis and recommendations for future studies. *Neuroscience Biobehavioral Reviews,* 107**,** 47-58.

BUNGERT, A., ANTUNES, A., ESPENHAHN, S. & THIELSCHER, A. 2017. Where does TMS stimulate the motor cortex? Combining electrophysiological measurements and realistic field estimates to reveal the affected cortex position. *Cerebral Cortex,* 27**,** 5083-5094.

CABEZA, R., CIARAMELLI, E. & MOSCOVITCH, M. 2012. Cognitive contributions of the ventral parietal cortex: an integrative theoretical account. *Trends in cognitive sciences,* 16**,** 338-352.

CHAMBERS, C. D., STOKES, M. G. & MATTINGLEY, J. B. 2004. Modality-specific control of strategic spatial attention in parietal cortex. *Neuron,* 44**,** 925-930.

CHICA, A. B., BARTOLOMEO, P. & VALERO-CABRÉ, A. 2011. Dorsal and ventral parietal contributions to spatial orienting in the human brain. *Journal of Neuroscience,* 31**,** 8143-8149.

CORBETTA, M., PATEL, G. & SHULMAN, G. 2008. The reorienting system of the human brain: from environment to theory of mind. *Neuron,* 58**,** 306-324.

CORBETTA, M. & SHULMAN, G. L. 2002. Control of goal-directed and stimulus-driven attention in the brain. *Nature reviews neuroscience,* 3**,** 201-215.

COX, R. W. & HYDE, J. S. 1997. Software tools for analysis and visualization of fMRI data. *NMR in Biomedicine: An International Journal Devoted to the Development Application of Magnetic Resonance In Vivo,* 10**,** 171-178.

DALE, A. M., FISCHL, B. & SERENO, M. I. 1999. Cortical surface-based analysis: I. Segmentation and surface reconstruction. *Neuroimage,* 9**,** 179-194.

DIEKHOFF, S., ULUDAĞ, K., SPARING, R., TITTGEMEYER, M., CAVUŞOĞLU, M., VON CRAMON, D. Y. & GREFKES, C. 2011. Functional localization in the human brain: Gradient-echo, spin-echo, and arterial spin-labeling fMRI compared with neuronavigated TMS. *Human brain mapping,* 32**,** 341-357.

DORICCHI, F., MACCI, E., SILVETTI, M. & MACALUSO, E. 2010. Neural correlates of the spatial and expectancy components of endogenous and stimulus-driven orienting of attention in the Posner task. *Cerebral Cortex,* 20**,** 1574-1585.

ESTEBAN, O., MARKIEWICZ, C. J., BLAIR, R. W., MOODIE, C. A., ISIK, A. I., ERRAMUZPE, A., KENT, J. D., GONCALVES, M., DUPRE, E. & SNYDER, M. 2019. fMRIPrep: a robust preprocessing pipeline for functional MRI. *Nature methods,* 16**,** 111-116.

FETSCH, C. R. 2016. The importance of task design and behavioral control for understanding the neural basis of cognitive functions. *Current opinion in neurobiology,* 37**,** 16-22.

GALLOTTO, S., SCHUHMANN, T., DUECKER, F., MIDDAG-VAN SPANJE, M., DE GRAAF, T. A. & SACK, A. T. 2022. Concurrent frontal and parietal network TMS for modulating attention. *Iscience,* 25**,** 103962.

GORGOLEWSKI, K., BURNS, C. D., MADISON, C., CLARK, D., HALCHENKO, Y. O., WASKOM, M. L. & GHOSH, S. S. 2011. Nipype: a flexible, lightweight and extensible neuroimaging data processing framework in python. *Frontiers in neuroinformatics***,** 13.

GREVE, D. N. & FISCHL, B. 2009. Accurate and robust brain image alignment using boundary-based registration. *Neuroimage,* 48**,** 63-72.

GROPPA, S., MUTHURAMAN, M., OTTO, B., DEUSCHL, G., SIEBNER, H. R. & RAETHJEN, J. 2013. Subcortical substrates of TMS induced modulation of the cortico-cortical connectivity. *Brain stimulation,* 6**,** 138-146.

GROSBRAS, M.-H. & PAUS, T. 2002. Transcranial magnetic stimulation of the human frontal eye field: effects on visual perception and attention. *Journal of cognitive neuroscience,* 14**,** 1109-1120.

HALLETT, M. 2000. Transcranial magnetic stimulation and the human brain. *Nature,* 406**,** 147-150.

HARTWIGSEN, G., BERGMANN, T. O., HERZ, D. M., ANGSTMANN, S.,

KARABANOV, A., RAFFIN, E., THIELSCHER, A. & SIEBNER, H. R. 2015. Modeling the effects of noninvasive transcranial brain stimulation at the biophysical, network, and cognitive level. *Progress in brain research,* 222**,** 261-287.

HARTWIGSEN, G. & SILVANTO, J. 2022. Noninvasive Brain Stimulation: Multiple Effects on Cognition. *The Neuroscientist***,** 10738584221113806.

HEDGE, C., POWELL, G. & SUMNER, P. 2018. The reliability paradox: Why robust cognitive tasks do not produce reliable individual differences. *Behavior research methods,* 50**,** 1166-1186.

IGELSTRÖM, K. M. & GRAZIANO, M. S. 2017. The inferior parietal lobule and temporoparietal junction: a network perspective. *Neuropsychologia,* 105**,** 70-83.

JAMADAR, S., HUGHES, M., FULHAM, W. R., MICHIE, P. T. & KARAYANIDIS, F. 2010. The spatial and temporal dynamics of anticipatory preparation and response inhibition in task-switching. *Neuroimage,* 51**,** 432-449.

JENKINSON, M., BANNISTER, P., BRADY, M. & SMITH, S. 2002. Improved optimization for the robust and accurate linear registration and motion correction of brain images. *Neuroimage,* 17**,** 825-841.

JOHNSON, A. & PROCTOR, R. W. 2004. *Attention: Theory and practice*, Sage.

KLEIN, A., GHOSH, S. S., BAO, F. S., GIARD, J., HÄME, Y., STAVSKY, E., LEE, N., ROSSA, B., REUTER, M. & CHAIBUB NETO, E. 2017. Mindboggling morphometry of human brains. *PLoS computational biology,* 13**,** e1005350.

KOCH, I., RUGE, H., BRASS, M., RUBIN, O., MEIRAN, N. & PRINZ, W. 2003. Equivalence of cognitive processes in brain imaging and behavioral studies: evidence from task switching. *Neuroimage,* 20**,** 572-577.

KRALL, S. C., VOLZ, L. J., OBERWELLAND, E., GREFKES, C., FINK, G. R. & KONRAD, K. 2016. The right temporoparietal junction in attention and social interaction: A transcranial magnetic stimulation study. *Human brain mapping,*

37**,** 796-807.

LAAKSO, I., MURAKAMI, T., HIRATA, A. & UGAWA, Y. 2018. Where and what TMS activates: experiments and modeling. *Brain Stimulation,* 11**,** 166-174.

LUNVEN, M. & BARTOLOMEO, P. 2017. Attention and spatial cognition: Neural and anatomical substrates of visual neglect. *Annals of physical rehabilitation medicine,* 60**,** 124-129.

MAKAROV, S. N., GOLESTANIRAD, L., WARTMAN, W. A., NGUYEN, B. T., NOETSCHER, G. M., AHVENINEN, J. P., FUJIMOTO, K., WEISE, K. & NUMMENMAA, A. 2021. Boundary element fast multipole method for modeling electrical brain stimulation with voltage and current electrodes. *Journal of neural engineering,* 18**,** 0460d4.

NATALE, E., MARZI, C. A. & MACALUSO, E. 2009. FMRI correlates of visuo-spatial reorienting investigated with an attention shifting double-cue paradigm. *Human Brain Mapping,* 30**,** 2367-2381.

NIELSEN, J. D., MADSEN, K. H., PUONTI, O., SIEBNER, H. R., BAUER, C., MADSEN, C. G., SATURNINO, G. B. & THIELSCHER, A. 2018. Automatic skull segmentation from MR images for realistic volume conductor models of the head: Assessment of the state-of-the-art. *Neuroimage,* 174**,** 587-598.

NIEMINEN, J. O., KOPONEN, L. M. & ILMONIEMI, R. J. 2015. Experimental characterization of the electric field distribution induced by TMS devices. *Brain stimulation,* 8**,** 582-589.

NUMSSEN, O., BZDOK, D. & HARTWIGSEN, G. 2021a. Functional specialization within the inferior parietal lobes across cognitive domains. *elife,* 10.

NUMSSEN, O., VAN DER BURGHT, C. L. & HARTWIGSEN, G. 2023. Revisiting the focality of non-invasive brain stimulation-implications for studies of human cognition. *Neuroscience Biobehavioral Reviews,* 105154.

NUMSSEN, O., ZIER, A.-L., THIELSCHER, A., HARTWIGSEN, G., KNÖSCHE, T. R. & WEISE, K. 2021b. Efficient high-resolution TMS mapping of the

human motor cortex by nonlinear regression. *NeuroImage,* 245**,** 118654.

OLDFIELD, R. C. 1971. The assessment and analysis of handedness: the Edinburgh inventory. *Neuropsychologia,* 9**,** 97-113.

PEELEN, M. V., HESLENFELD, D. J. & THEEUWES, J. 2004. Endogenous and exogenous attention shifts are mediated by the same large-scale neural network. *Neuroimage,* 22**,** 822-830.

PERERA, T., GEORGE, M. S., GRAMMER, G., JANICAK, P. G., PASCUAL-LEONE, A. & WIRECKI, T. S. 2016. The clinical TMS society consensus review and treatment recommendations for TMS therapy for major depressive disorder. *Brain stimulation,* 9**,** 336-346.

POSNER, M. I. 1980. Orienting of attention. *Quarterly journal of experimental psychology,* 32**,** 3-25.

POWER, J. D., BARNES, K. A., SNYDER, A. Z., SCHLAGGAR, B. L. & PETERSEN, S. E. 2012. Spurious but systematic correlations in functional connectivity MRI networks arise from subject motion. *Neuroimage,* 59**,** 2142-2154.

POWER, J. D., MITRA, A., LAUMANN, T. O., SNYDER, A. Z., SCHLAGGAR, B. L. & PETERSEN, S. E. 2014. Methods to detect, characterize, and remove motion artifact in resting state fMRI. *Neuroimage,* 84**,** 320-341.

PROSKOVEC, A. L., HEINRICHS-GRAHAM, E., WIESMAN, A. I., MCDERMOTT, T. J. & WILSON, T. W. 2018. Oscillatory dynamics in the dorsal and ventral attention networks during the reorienting of attention. *Human brain mapping,* 39**,** 2177-2190.

RAWJI, V., LATORRE, A., SHARMA, N., ROTHWELL, J. C. & ROCCHI, L. 2020. On the use of TMS to investigate the pathophysiology of neurodegenerative diseases. *Frontiers in neurology,* 11**,** 584664.

RUSHWORTH, M. F., ELLISON, A. & WALSH, V. 2001. Complementary localization and lateralization of orienting and motor attention. *Nature neuroscience,* 4**,** 656-661.

SATURNINO, G. B., MADSEN, K. H. & THIELSCHER, A. 2019. Electric field simulations for transcranial brain stimulation using FEM: an efficient implementation and error analysis. *Journal of neural engineering,* 16**,** 066032.

SCHUWERK, T., SCHURZ, M., MÜLLER, F., RUPPRECHT, R. & SOMMER, M. 2017. The rTPJ's overarching cognitive function in networks for attention and theory of mind. *Social cognitive and affective neuroscience,* 12**,** 157-168.

SEGAL, E. & PETRIDES, M. 2012. The morphology and variability of the caudal rami of the superior temporal sulcus. *European Journal of Neuroscience,* 36**,** 2035-2053.

SHULMAN, G. L., ASTAFIEV, S. V., FRANKE, D., POPE, D. L., SNYDER, A. Z., MCAVOY, M. P. & CORBETTA, M. 2009. Interaction of stimulus-driven reorienting and expectation in ventral and dorsal frontoparietal and basal ganglia-cortical networks. *Journal of Neuroscience,* 29**,** 4392-4407.

SMALL, D. M., GITELMAN, D. R., GREGORY, M. D., NOBRE, A. C., PARRISH, T. B. & MESULAM, M.-M. 2003. The posterior cingulate and medial prefrontal cortex mediate the anticipatory allocation of spatial attention. *Neuroimage,* 18**,** 633-641.

SZCZEPANSKI, S. M., PINSK, M. A., DOUGLAS, M. M., KASTNER, S. & SAALMANN, Y. B. 2013. Functional and structural architecture of the human dorsal frontoparietal attention network. *Proceedings of the National Academy of Sciences,* 110**,** 15806-15811.

THIEL, C. M., ZILLES, K. & FINK, G. R. 2004. Cerebral correlates of alerting, orienting and reorienting of visuospatial attention: an event-related fMRI study. *Neuroimage,* 21**,** 318-328.

THIELSCHER, A., ANTUNES, A. & SATURNINO, G. B. Field modeling for transcranial magnetic stimulation: A useful tool to understand the physiological effects of TMS? 2015 37th annual international conference of the IEEE engineering in medicine and biology society (EMBC), 2015. IEEE, 222-225.

TUSTISON, N. J., AVANTS, B. B., COOK, P. A., ZHENG, Y., EGAN, A., YUSHKEVICH, P. A. & GEE, J. C. 2010. N4ITK: improved N3 bias correction. *IEEE transactions on medical imaging,* 29**,** 1310-1320.

VAN HOORNWEDER, S., MEESEN, R. & CAULFIELD, K. A. 2022. On the importance of using both T1-weighted and T2-weighted structural magnetic resonance imaging scans to model electric fields induced by non-invasive brain stimulation in SimNIBS. *Brain Stimulation,* 15**,** 641-644.

VAN MAANEN, L., FORSTMANN, B. U., KEUKEN, M. C., WAGENMAKERS, E.-J. & HEATHCOTE, A. 2016. The impact of MRI scanner environment on perceptual decision-making. *Behavior research methods,* 48**,** 184-200.

VOSSEL, S., GENG, J. J. & FINK, G. R. 2014. Dorsal and ventral attention systems: distinct neural circuits but collaborative roles. *The Neuroscientist,* 20**,** 150-159.

WAGNER, T., GANGITANO, M., ROMERO, R., THÉORET, H., KOBAYASHI, M., ANSCHEL, D., IVES, J., CUFFIN, N., SCHOMER, D. & PASCUAL-LEONE, A. 2004. Intracranial measurement of current densities induced by transcranial magnetic stimulation in the human brain. *Neuroscience letters,* 354**,** 91-94.

WALSH, V. & COWEY, A. 2000. Transcranial magnetic stimulation and cognitive neuroscience. *Nature Reviews Neuroscience,* 1**,** 73-80.

WANG, J., ZHANG, J., RONG, M., WEI, X., ZHENG, D., FOX, P. T., EICKHOFF, S. B. & JIANG, T. 2016. Functional topography of the right inferior parietal lobule structured by anatomical connectivity profiles. *Human brain mapping,* 37**,** 4316-4332.

WEISE, K., NUMSSEN, O., KALLOCH, B., ZIER, A. L., THIELSCHER, A., HAUEISEN, J., HARTWIGSEN, G. & KNÖSCHE, T. R. 2023. Precise motor mapping with transcranial magnetic stimulation. *Nature protocols,* 18**,** 293-318.

WEISE, K., NUMSSEN, O., THIELSCHER, A., HARTWIGSEN, G. & KNÖSCHE, T. R. 2020. A novel approach to localize cortical TMS effects. *Neuroimage,*

209**,** 116486.

WILLIAMS, K. A., NUMSSEN, O. & HARTWIGSEN, G. 2022. Task-specific network interactions across key cognitive domains. *Cerebral Cortex,* 32**,** 5050-5071.

ZHANG, Y., BRADY, M. & SMITH, S. 2001. Segmentation of brain MR images through a hidden Markov random field model and the expectation-maximization algorithm. *IEEE transactions on medical imaging,* 20**,** 45-57.